ADVANCED MATERIALS

SThM probe would have provided a low-resistance path from the cathode to earth. The SThM system was used to measure surface temperature by placing the probe in contact with the surface of the LED cathode. The SThM probe (an ultra-miniaturized resistance temperature detector) was constructed from Wollaston wire consisting of a 75 μm diameter silver wire with a 5 μm diameter 90 % platinum/10 % rhodium core. The wire was made into a loop with a radius of curvature of about 30°. Where the loop was formed, the silver was etched away revealing the platinum/rhodium core. The two silver arms formed a cantilever structure across which a mirror was attached for force monitoring using laser beam deflection. The probe was mounted on an Explorer scanning probe microscope manufactured by Veeco. The LED was mounted on the Explorer microscope stage on a magnetic metal plate using a small quantity of superglue.

To calibrate the SThM probe, it was first placed in contact with a calibrated hot stage, and the voltage output from the probe was measured at a series of different hot-stage temperatures. The SThM was then used to measure the temperature at the centre of each LED pixel as a current–voltage scan was recorded. The centre of the LED was first located by using the SThM to create a topographic map of the surface. The probe was then moved to the centre of the device and a current–voltage–temperature ramp was recorded at approximately 10 s per voltage interval. As discussed in the text, the LEDs reached their final operating temperature in a time of 4 s or less. The temporal resolution of the SThM system in our experimental configuration was ~ 0.25 s, thus the temperature recorded by the SThM in a current–voltage–temperature measurement can be considered as an equilibrium temperature for each particular power input. Note that all measurements were made in air.

Current–voltage–luminance measurements were also made on a series of representative LEDs using in a nitrogen-filled glove-box. Luminance was measured from standard area LEDs using a calibrated luminance meter. The luminance of the small area LEDs was measured using a photodiode, which had been previously calibrated against a standard-area LED operating at a known brightness. A correction factor was applied to the photodiode response function to account for the difference in emissive areas between the small area and standard area devices.

The external quantum efficiency (ϕ_{Ext}) (photons per injected charge) was determined from the LED efficiency (in terms of cd A^{-1}) using a photo-optic conversion factor [26]. The external power efficiency (P) was calculated [27] using $P = \phi_{Ext} E_p / eV_{LED}$, where E_p is the EL photon energy in Joules and V_{LED} is the applied LED bias.

Received: September 5, 2003
Final Version: November 4, 2003

[1] O. Gelsen, *Opto Laser Eur.* **2003**, *107*, 33.
[2] J. R. Sheats, H. Antoniadis, M. Hueschen, W. Leonard, J. Miller, R. Moon, D. Roitman, A. Stocking, *Science* **1996**, *273*, 884.
[3] T. Mori, T. Mitsuoka, M. Ishii, H. Fujikawa, Y. Taga, *Appl. Phys. Lett*. **2002**, *80*, 3895.
[4] P. N. M. dos Anjos, H. Aziz, N. X. Hu, Z. D. Popovic, *Org. Electron*. **2002**, *2*, 9.
[5] J. S. Kim, R. H. Friend, F. Cacialli, *Appl. Phys. Lett*. **1999**, *74*, 3084.
[6] N. Tessler, N. T. Harrison, D. S. Thomas, R. H. Friend, *Appl. Phys. Lett*. **1998**, *73*, 732.
[7] J. M. Lupton, *Appl. Phys. Lett*. **2002**, *80*, 186.
[8] N. Tessler, *Adv. Mater*. **1999**, *11*, 363.
[9] X. Zhou, J. He, L. S. Liao, M. Lu, X. M. Ding, X. Y. Hou, X. M. Zhang, X. Q. He, S. T. Lee, *Adv. Mater.* **2000**, *12*, 265.
[10] C. I. Wilkinson, D. G. Lidzey, L. C. Pallilis, R. B. Fletcher, S. J. Martin, X. H. Wang, D. D. C. Bradley, *Appl. Phys. Lett*. **2001**, *79*, 171.
[11] J. C. Sturm, W. Wilson, M. Iodice, *IEEE J. Sel. Top. Quantum Electron*. **1998**, *4*, 75.
[12] A. Majumdar, *Annu. Rev. Mater. Sci*. **1999**, *29*, 505.
[13] H. M. Pollock, A. Hammiche, *J. Phys. D: Appl. Phys*. **2001**, *34*, R23.
[14] T. H. Lee, X. Guo, G. D. Shen, Y. Ji, G. H. Wang, J. Y. Du, X. Z. Wang, G. Gao, A. Altes, L. J. Balk, J. C. H. Phang, *Microelectron. Reliab*. **2002**, *42*, 1711.
[15] K. Luo, R. W. Herrick, A. Majumdar, P. Petroff, *Appl. Phys. Lett*. **1997**, *71*, 1604.
[16] Z. Xie, L. Han, F. Wei, X. Wang, Y. Gu, H. Chen, *Mater. Sci. Eng.* **2000**, *A292*, 179.
[17] A. Majumdar, J. P. Carrejo, J. Lai, *Appl. Phys. Lett*. **1993**, *62*, 2501.
[18] R. Heiderhoff, M. Palaniappan, J. C. H. Phang, L. J. Balk, *Microelectron. Reliab*. **2000**, *40*, 1383.
[19] M. Redecker, D. D. C. Bradley, M. Inbasekaran, E. P. Woo, *Appl. Phys. Lett*. **1998**, *73*, 1565.
[20] A. J. Campbell, D. D. C. Bradley, H. Antoniadis, *Appl. Phys. Lett*. **2001**, *79*, 2133.
[21] J. Morgado, R. H. Friend, F. Cacialli, *Appl. Phys. Lett.* **2002**, *80*, 2436.
[22] C. Adachi, M. A. Baldo, M. E. Thompson, S. R. Forrest, *J. Appl. Phys*. **2001**, *90*, 5048.
[23] K. P. Pipe, J. R. J. Ram, *IEEE Photonic. Tech. L*. **2003**, *15*, 504.
[24] L. A. Coldren, S. W. Corzine, *Diode Lasers and Photonic Integrated Circuits*, Wiley, New York **1995**, p. 56.
[25] M. S. Weaver, L. A. Michalski, K. Rajan , M. A. Rothman, J. A. Silvernail, J. J. Brown, P. E. Burrows, G. L. Graff, M. E. Gross, P. M. Martin, M. Hall, E. Mast, C. Bonham, W. Bennett, M. Zumhoff, *Appl. Phys. Lett*. **2002**, *81*, 2929.
[26] T. Virgili, D. G. Lidzey, D. D. C. Bradley, *Adv. Mater*. **2000**, *12*, 58.
[27] J. C. Scott, G. G. Malliaras, in *Semiconducting Polymers* (Eds: G. Hadziioannou, P. F. Hutten), Wiley-VCH, Weinheim **1999**, Ch. 13.

Novel Nanostructured Electrodes for Solid Oxide Fuel Cells Fabricated by Combustion Chemical Vapor Deposition (CVD)**

By *Ying Liu*, *Shaowu Zha*, and *Meilin Liu**

Low-temperature solid oxide fuel cells (SOFCs) have attracted much attention in recent years because of their potential to dramatically reduce the cost of the materials and cell fabrication in addition to improved reliability, portability, and operational life.[1–6] To lower the resistance of dense electrolyte membranes at lower operating temperatures, either the thickness of traditional YSZ (8 mol-% Y_2O_3–ZrO_2) electrolyte must be reduced or alternate electrolyte materials with much high conductivities at low temperatures (such as doped ceria and lanthanum gallate) must be used. Meanwhile, the performance of electrodes (both anode and cathode) must be significantly improved to reduce the operating temperature,

[*] Prof. M. Liu, Y. Liu, Dr. S. Zha
School of Materials Science and Engineering
Georgia Institute of Technology
Atlanta, GA 30332-0245 (USA)
E-mail: meilin.liu@mse.gatech.edu

[**] This work was supported by the US Department of Energy–National Energy Technology Laboratory [Grant DE-FG26-01NT41274 and DE-F926-02NT41572] and by the Georgia Institute of Technology Molecular Design Institute under prime contract N00014-95-1-1116 from the Office of Naval Research.

  DOI: 10.1002/adma.200305767

either through development of new materials or creation of novel structures. It has been demonstrated that the viability to operate an SOFC at low temperatures is determined primarily by the cathode/electrolyte interface, since its polarization resistance increases rapidly as the temperature is decreased.[7] The work reported in this communication aims at developing novel nanostructured electrodes of extremely low interfacial polarization resistances by a versatile and cost-effective method, combustion chemical vapor deposition (CVD), in an effort to significantly reduce the operating temperature. This is a critical step toward making SOFCs affordable for a wide variety of applications.

An SOFC is an all-solid-state device that converts the chemical energy of fuels (such as hydrogen, natural gas, and other hydrocarbon fuels) directly to electricity with the highest energy efficiency and minimal pollutant emission. It is desirable to have a porous structure of mixed-conducting electrodes for fast transport of ionic and electronic defects through the solid phase, rapid flow of gases through the pores, and for efficient electrochemical reactions at the interfaces.[8–10] For example, in a Ni–$Ce_{0.9}Gd_{0.1}O_{1.95}$ (GDC) composite anode, Ni acts as both the catalyst and the electronic conducting phase, while GDC acts mainly as a matrix to support the catalyst and prohibit the metal from agglomeration under operating conditions. Ceria is reported to improve the anode catalytic activity as well, especially in SOFCs using hydrocarbon fuels.[11,12] It has been demonstrated that the length of the triple-phase boundary (TPB) correlates well with the interfacial resistances to electrochemical oxidation of hydrogen at the anode and reduction of oxygen at the cathode; thus, the extension of the TPB or the number of active reaction sites becomes a determining factor in improving electrode performance. This can be achieved by developing electrode materials of higher ambipolar conductivity and/or optimizing the architecture/microstructure of the electrodes. Consequently, extensive efforts have been devoted to searching for alternative cathode materials such as the composites consisting of $La_{0.6}Sr_{0.4}Co_{0.2}Fe_{0.8}O_{3-\delta}$ (LSCF), $Sm_{0.5}Sr_{0.5}CoO_{3-\delta}$ (SSC), and $Ce_{0.9}Gd_{0.1}O_{1.95}$ (GDC) or YSZ.[13,14] While considerable progress has been made on developing new electrode materials, little has been reported in cell performance enhancement by optimizing microstructure of the electrodes through new electroding processes. Although there is little argument that the creation of nanostructured electrodes with finer grain size could considerably improve the performance of fuel cells, especially at lower operating temperatures, the major technical challenge is how to fabricate the designed microstructure cost-effectively.

Combustion CVD is an open-air, flame-assisted chemical deposition process, capable of producing a wide range of coating morphologies from very dense to highly porous structures.[15,16] In liquid fuel combustion CVD, chemical precursors of the electrode materials are dissolved in a flammable organic solvent. The resulting solution is nebulized and the resulting aerosol is then combusted in open air, depositing a layer of porous electrodes onto an electrolyte substrate placed within tip region of the flame. Electrode compositions can be easily controlled by simply adjusting the ratios of the various chemical precursors in the solution. This technique is cost-effective because it uses inexpensive precursors (e.g., nitrates and metal–organics) and needs neither a furnace nor a vacuum chamber, which are costly and essential for conventional CVD processes. Moreover, the combustion CVD process, like other CVD processes, is insensitive to and has no specific requirement for the flatness of the substrate. It has been demonstrated that the combustion CVD process can be employed to prepare either nanosized powders or a variety of nanostructured films with controllable thickness and porosity.[17] A technique similar to combustion CVD has been used on the $La_{1-x}Sr_xMnO_{3-\delta}$ (LSM)/YSZ system earlier.[18–20] Interfacial resistances of the resulting electrodes were reported comparable to those fabricated by conventional techniques. Unfortunately, only symmetrical cells, not functional full cells, were fabricated and tested using that technique. In addition, there was no attempt to fabricate ceria-based SOFC systems, the performance of which is more sensitive to interfacial resistances because the intended operating temperature is low. For example, for a SOFC based on a 26 μm thick GDC electrolyte, Ni-GDC/GDC/SSC-GDC, the electrolyte resistances were reported to be 0.96 $\Omega\,cm^2$ and 0.67 $\Omega\,cm^2$ at 450 °C and 500 °C, respectively, while the interfacial polarization resistances were 5.2 $\Omega\,cm^2$ and 1.8 $\Omega\,cm^2$, much higher than the bulk electrolyte resistances.[21] Thus, reducing interfacial polarization resistances is the most effective way of enhancing the performances of low-temperature SOFCs.

In this communication, we report our recent advance in fabrication of functional SOFCs by depositing both cathode (70 wt.-% $Sm_{0.5}Sr_{0.5}CoO_{3-\delta}$ and 30 wt.-% $Sm_{0.1}Ce_{0.9}O_{3-\delta}$ (SDC)) and anode (70 wt.-% Ni and 30 wt.-% $Sm_{0.1}Ce_{0.9}O_{3-\delta}$) on 250 μm thick GDC electrolyte pellets using a combustion CVD process. Figure 1a shows a cross-sectional view of a fuel cell supported by a 250 μm thick GDC electrolyte membrane with combustion CVD-fabricated NiO–SDC anode (top layer) and SSC–SDC cathode (bottom layer). Both electrodes are relatively uniform with thickness of about 40 μm. The micrographs shown in Figures 1b,c reveal that both anodes and cathodes are highly porous and appear to adhere well to the electrolyte. The agglomerate size appears to be smaller for the anode than for the cathode. However, higher magnification scanning electron microscopy (SEM) images, shown in Figures 1d,e, reveal that each agglomerate actually consists of much smaller grains of about 50 nm in diameter. The primary grain sizes are also smaller for the anode than for the cathode. These nanostructured electrodes have extremely high surface area and are expected to significantly improve the electrochemical functionality.

Shown in Figure 2 are the X-ray diffraction (XRD) patterns of as-prepared cathodes and anodes, indicating that the composite anode consists of NiO and SDC phases whereas the cathode is composed of SSC and SDC phases.

Shown in Figure 3a are the impedance spectra of the fuel cell measured at 500 °C and 600 °C under open-circuit condi-

ADVANCED MATERIALS

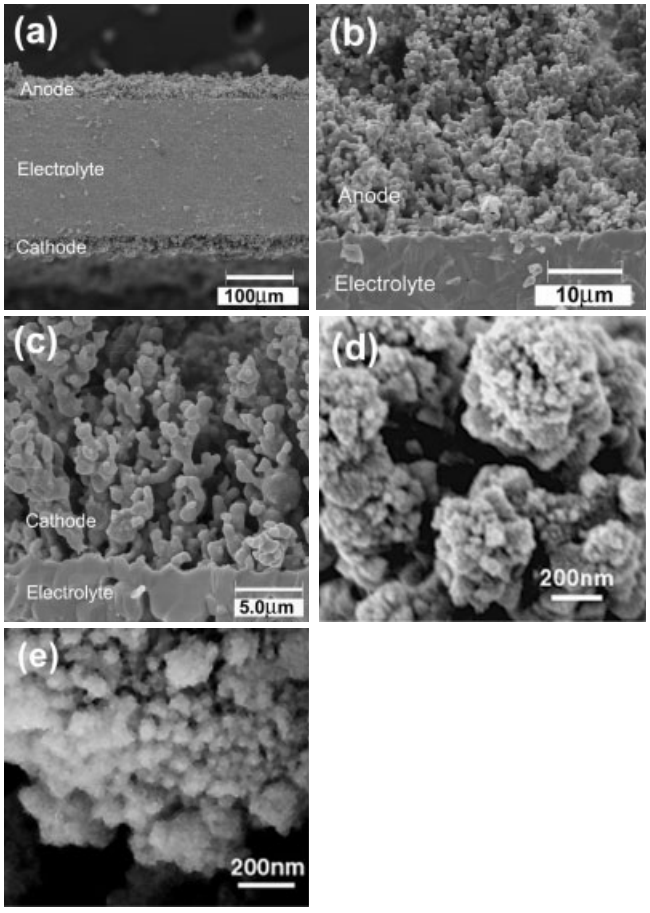

Figure 1. Cross-sectional views of an SOFC with both anode and cathode fabricated using combustion CVD: a) the entire cell with Ni-SDC anode, GDC electrolyte, and SSC–SDC cathode, b) anode–electrolyte interface, c) cathode–electrolyte interface, d) higher magnification of Ni-SDC composite anode, and e) higher magnification of SSC–SDC composite cathode.

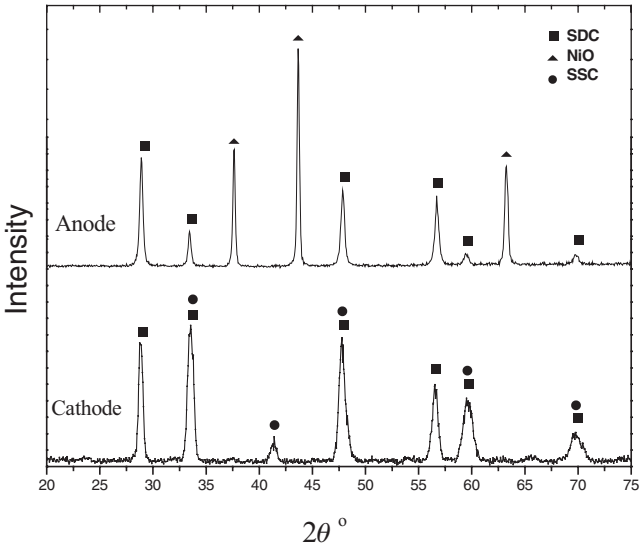

Figure 2. X-ray diffraction patterns of the anode (70 wt.-% Ni and 30 wt.-% SDC) and the cathode (70 wt.-% SSC and 30 wt.-% SDC) fabricated using combustion CVD.

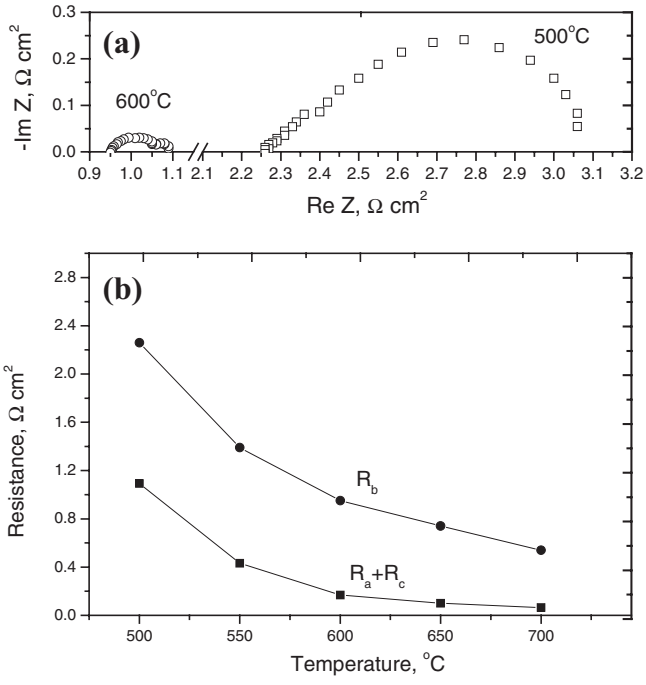

Figure 3. a) Impedance spectra of a single fuel cell as measured using a two-electrode configuration, and b) the bulk electrolyte and interfacial polarization resistances obtained from impedance spectra acquired at different temperatures.

tions using a two-electrode configuration. Since the electronic conduction in GDC is not negligible under the fuel cell conditions,[22] the bulk resistance of the electrolyte (R_b) and the polarization resistances of the electrode–electrolyte interfaces (R_a+R_c) can no longer be determined just from the impedance data. The combination of impedance measurement and open-circuit voltage (OCV) measurement becomes necessary to correct the partial shorting effect due to electronic conduction of GDC. Shown in Figure 3b are the electrolyte resistances (R_b) and the total interfacial resistances (R_a+R_c) as calculated from the impedance data and OCV measurements.[23] The electrode–electrolyte interfacial polarization resistance is estimated to be 1.09 Ω cm^2 at 500 °C, 0.43 Ω cm^2 at 550 °C, and 0.17 Ω cm^2 at 600 °C, respectively.

Shown in Figure 4 are the polarization resistances of the cell with electrodes fabricated by combustion CVD, together with data reported in literature for doped ceria-based SOFCs. While some of the data[13,14] were obtained using symmetrical cells, they should be comparable to those obtained from fuel cells if correctly analyzed;[23] i.e., taking into consideration of partial shorting due to electronic conduction of the electrolyte GDC under functional cell conditions. Clearly, the fuel cell with electrodes fabricated by combustion CVD displayed much lower interfacial polarization resistances than those prepared by conventional methods: slurry painting,[13] spin-coating,[14] and screen printing.[21] The observed interfacial polar-

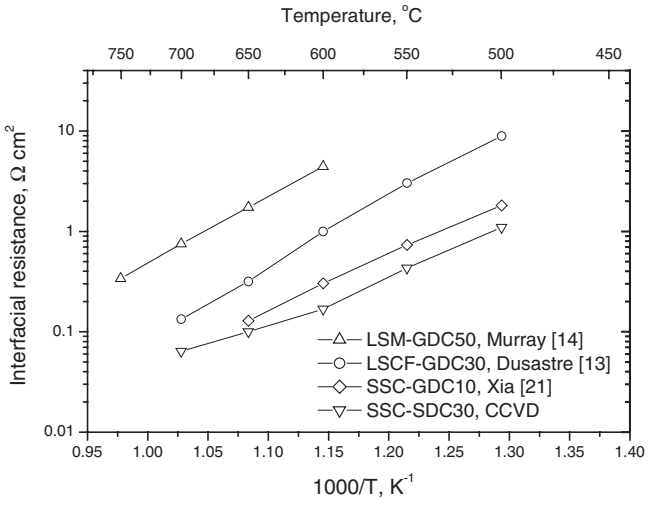

Figure 4. Comparison of interfacial polarization resistances as determined from impedance spectra for electrodes fabricated using different techniques: slurry painting [13], spin-coating [14], and screen printing [21].

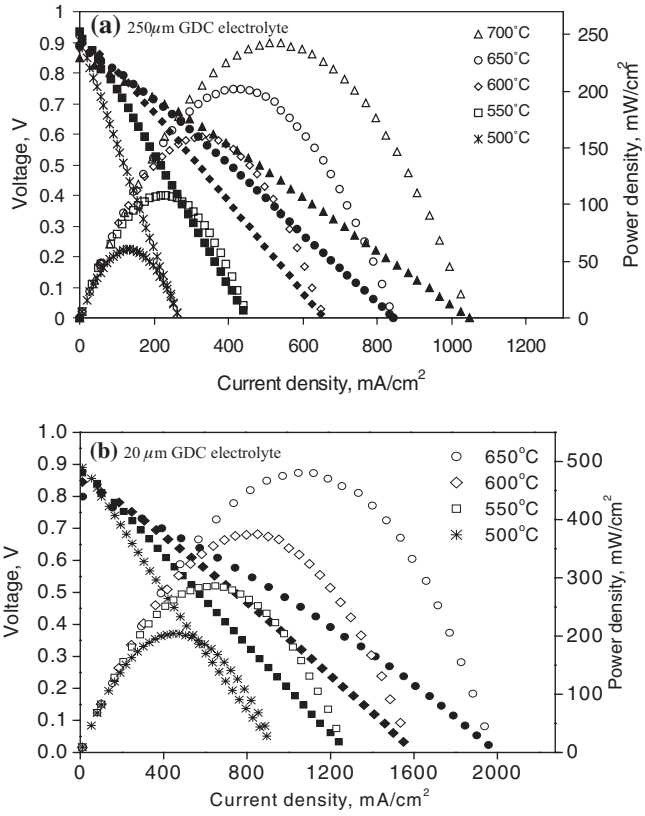

Figure 5. Cell voltages and power densities as a function of current density for fuel cells with: a) both cathode (SSC–SDC) and anode (Ni-SDC) fabricated using combustion CVD on a GDC electrolyte membrane with thickness of 250 μm, and b) a combustion CVD-fabricated cathode (SSC-SDC) on a 20 μm thick GDC electrolyte film supported by Ni-GDC anode fabricated by dry-pressing and co-firing.

ization resistances of the electrodes fabricated by combustion CVD represent the lowest ever reported for these cathode/electrolyte systems.

Shown in Figure 5a are the cell voltages and power densities as a function of current density for a single cell with both anode and cathode fabricated by combustion CVD. The maximum power densities are 60, 108, 159, 202, and 243 mW cm^{-2} at 500, 550, 600, 650, and 700 °C, respectively. These are impressive performance data for a fuel cell based on an electrolyte 250 μm thick. As revealed from impedance spectra shown in Figure 3a, electrolyte resistances were much higher than the electrode–electrolyte interfacial polarization resistance and, thus, the cell performance was mainly limited by the electrolyte resistance. To further demonstrate the benefit brought about by low interfacial polarization resistances, anode-supported half cells with 20 μm thick GDC electrolytes were fabricated by a dry-pressing and co-firing process as described elsewhere.[21] Subsequently, SSC–SDC cathodes were fabricated on the GDC electrolyte films (supported by anode) using combustion CVD. As expected, much higher powder densities were achieved for an anode-supported cell with a 20 μm thick GDC electrolyte. The peak power densities are 204, 286, 375, and 481 mW cm^{-2} at 500, 550, 600, and 650 °C, respectively, as shown in Figure 5b.

Highly porous and nanostructured electrodes for low-temperature SOFCs have been successfully fabricated using a combustion CVD process. The electrodes fabricated by combustion CVD consist of nano-grains of about 50 nm, exhibiting extremely high surface area and remarkably low polarization resistances. XRD patterns confirmed the formation of desired crystalline phases for as-prepared NiO–SDC anodes and SSC–SDC cathodes. It is evident that combustion CVD is a highly effective approach to fabrication of high-performance electrodes for low-temperature SOFCs, producing the lowest interfacial polarization resistances (1.09 Ω cm^2 at 500 °C, and 0.17 Ω cm^2 at 600 °C) ever reported for the cathode materials. An anode supported cell with a 20 μm thick electrolyte demonstrated a power density of 375 mW cm^{-2} at 600 °C. Little deterioration in either microstructure or performance was observed after 172 h of operation. While the long-term stability of these electrodes is yet to be determined, the results indicate a new direction to significantly improve the performance of low temperature SOFCs. The high deposition rate, short deposition time, and high-temperature deposition conditions result in nanosized grains, superior bonding to electrolyte, and desired crystalline phases, which are important attributes needed to achieve low interfacial polarization resistances, high power densities, and potentially lower operating temperatures.

Experimental

Detailed description of combustion CVD apparatus used for this study is available elsewhere [17]. Metal nitrates of Sr, Sm, Co, Ce, and

ADVANCED MATERIALS

Ni were obtained from Aldrich. Solutions were prepared by dissolving stoichiometric amounts of precursors into an organic solvent and agitated by a magnetic stirring bar until completely dissolved. Methane was used as the fuel gas and oxygen served as the oxidizer for the combustion flame.

Dense GDC ($Gd_{0.1}Ce_{0.9}O_{1.95}$) pellets of 10 mm diameter and 250 μm thickness were prepared by a dry-pressing process and sintered at 1350 °C for 5 h to achieve relative density of greater than 96 %. Before deposition, the GDC substrates were held at the tip position of flame for 7 min. After deposition of each electrode, the precursor solution was switched, and substrates were turned over for deposition of the other electrode material. Anode supported half cells were fabricated by a co-firing process. The dry-pressed Ni-GDC/GDC bilayer pellets were co-sintered at 1350 °C for 5 h, resulting in an GDC film of about 20 μm on a Ni-GDC substrate.

The microscopic features of the prepared electrodes were characterized using a scanning electron microscope (SEM, Hitachi S-800) with an energy dispersive spectroscopy (EDS) attachment. Electrochemical performances of the cells were measured at 500–700 °C with humidified (3 vol.-% water) hydrogen as fuel and stationary air as oxidant at ambient pressure. Impedances were measured in the frequency range from 0.01 Hz to 100 KHz with an EG&G Potentiostat/Galvanostat (Model 273 A) and lock-in amplifier (5210).

Received: July 30, 2003
Final version: October 29, 2003

[1] N. Q. Minh, *J. Am. Ceram. Soc.* **1993**, *76*, 563.
[2] C. Xia, M. Liu, *J. Am. Chem. Soc.* **2001**, *84*, 1903.
[3] S. de. Souza, S. J. Visco, L. C. DeJonghe, *J. Electrochem. Soc.* **1997**, *144*, L35.
[4] T. Suzuki, I. Kosacki, H. U. Anderson, *Solid State Ionics* **2002**, *151*, 111.
[5] B. C. H. Steele, *Solid State Ionics* **2000**, *129*, 95.
[6] S. C. Singhal, *Solid State Ionics* **2002**, *152–153*, 405.
[7] C. Xia, M. Liu, *Adv. Mater.* **2002**, *14*, 521.
[8] M. Dokiya, *Solid State Ionics* **2002**, *152–153*, 383.
[9] E. Ivers-Tiffee, A. Weber, D. Herbstritt, *J. Eur. Ceram. Soc.* **2001**, *21*, 1805.
[10] C. W. Tanner, K. Z. Fung, A. V. Virkar, *J. Electrochem. Soc.* **1997**, *144*, 21.
[11] S. Park, J. M. Vohs, R. J. Gorte, *Nature* **2000**, *404*, 265.
[12] E. P. Murray, T. Tsai, S. A. Barnett, *Nature* **1999**, *400*, 649.
[13] V. Dusastre, J. A. Kilner, *Solid State Ionics* **1999**, *126*, 163.
[14] E. P. Murray, S. A. Barnett, *Solid State Ionics* **2001**, *143*, 265.
[15] A. T. Hunt, W. B. Carter, J. K. Cochran, *Appl. Phys. Lett.* **1993**, *63*, 266.
[16] A. T. Hunt, J. K. Cochran, W. R. Carter, *US Patent 5 652 021*, **1997**.
[17] Y. Liu, W. Rauch, M. Liu, in *Solid State Ionic Devices III* (Eds: E. Wachsman, K. Swider-Lyons, M. F. Carolan, F. H. Garzon, M. Liu, J. R. Setter), The Electrochemical Society, Pennington, NJ **2002**, p. 215.
[18] K. L. Choy, S. Charojrochkul, B. C. H. Steele, *Solid State Ionics* **1997**, *96*, 49.
[19] K. Choy, W. Bai, S. Charojrochkul, B. C. H. Steele, *J. Power Sources* **1998**, *71*, 361.
[20] S. Charojrochkul, K. L. Choy, B. C. H. Steele, *Solid State Ionics* **1999**, *121*, 107.
[21] C. Xia, M. Liu, *Solid State Ionics* **2001**, *144*, 249.
[22] M. Liu, A. Joshi, in *Ionic and Mixed Conducting Ceramics* (Eds: T. A. Ramanarayanan, H. L. Tuller), Vol. 91-12, The Electrochemical Society, Pennington, NJ **1991**, p. 191.
[23] M. Liu, H. Hu, *J. Electrochem. Soc.* **1996**, *143*, L109.

Nanocarving of Bulk Titania Crystals into Oriented Arrays of Single-Crystal Nanofibers via Reaction with Hydrogen-Bearing Gas**

By *Sehoon Yoo*, *Sheikh A. Akbar*,* *Kenneth H. Sandhage*

Appreciable worldwide activity is underway to develop new advanced materials and devices with controlled features on the nanometer scale.[1] Owing to attractive electronic, photocatalytic, gas-sensing, and antimicrobial properties, nanostructured titanium oxide-based materials (e.g., nanowires, nanotubes, or nanoporous structures) are receiving significant attention.[2] However, the widespread utilization of such advanced nanostructured materials is often complicated by the conflicting demands for precise control of fine features (down to the nanometer scale) and for large-scale mass production (up to the tonnage scale). Therefore, novel methods for fabricating well-organized titanium oxide nanostructures that are simple (i.e., that involve a minimal number of steps) and that can be readily scaled up (via continuous processing operations) need to be identified to allow for rapid and low-cost manufacturing.

In this paper, a surprisingly simple and easily scalable method has been discovered for "carving" oriented arrays of single-crystal titania nanofibers from bulk titania crystals: reaction with a hydrogen-bearing gas. The bulk crystals undergoing such reaction were present on the external surfaces of dense, polycrystalline titanium oxide disks. The disks were prepared by heating titanium oxide powder compacts for 6 h at 1200 °C in air. X-ray diffraction (XRD) analyses of the disk-shaped specimens revealed peaks for only the rutile polymorph of titanium oxide (Fig. 1A). After the 1200 °C heat treatment, the disks had bulk densities of 4035 ± 85 kg/m^3, which corresponded to 94.9 ± 2.0 % of the theoretical density of rutile (4250 kg/m^3).[3] Secondary electron images of the surfaces of the polycrystalline rutile specimens are shown in Figures 2A,B. These images reveal distinct facets on, and distinct boundaries between, the rutile grains. The average size of the rutile grains was 4 μm. The dense rutile disks were exposed to a flowing 5 % H_2/95 % N_2 gas mixture at 700 °C for 8 h. Secondary electron images of the external surface of a rutile spec-

[*] Prof. S. A. Akbar, S. Yoo
Center for Industrial Sensors and Measurements (CISM)
Department of Materials Science and Engineering
The Ohio State University
Columbus, OH 43210 (USA)
E-mail: Akbar@mse.eng.ohio-state.edu
Prof. K. H. Sandhage
School of Materials Science and Engineering
Georgia Institute of Technology
Atlanta, GA 30332-0245 (USA)

[**] This work was supported by the U.S. National Science Foundation.

  DOI: 10.1002/adma.200305781